



Diffusion pack cementation of hafnium powder with halide activator on Ni–Ti shape memory alloy

Seung Yong Yang¹ · YeounJu Kwon² · Seong-Woo Choi³ · Jeoung Han Kim²

Received: 1 July 2017 / Accepted: 15 December 2017 / Published online: 28 December 2017
© Akadémiai Kiadó, Budapest, Hungary 2017

Abstract

The effect of a Hf chloride activator on the pack cementation of Hf powder on a Ni–Ti shape memory alloy wire was investigated. For this purpose, a Ni–Ti wire with a diameter of 0.5 mm was pack cemented in a powder mixture consisting of Hf and HfCl₄ powders at 1000 °C for 24 h. It was observed that Hf noticeably diffused into the Ni–Ti matrix with the aid of the HfCl₄ activator. The diffusion distance significantly increased as the amount of HfCl₄ activator increased. By the addition of 10 mass% HfCl₄, the martensite-to-austenite phase transformation start and finish temperatures increased from 12 to 142 °C and from 28 to 200 °C, respectively. The diffusion kinetics model was established based on Fick's first law. It is suggested that 48 h of halide-activated pack cementation with 10 wt% HfCl₄ is necessary to increase the overall Hf content above 15 at.% throughout the Ni–Ti wire.

Keywords Shape memory alloy · Ni–Ti · Pack cementation · Diffusion · Hafnium

Introduction

Binary Ni–Ti alloys are very attractive materials because of their superior super-elasticity and shape memory effect as compared to other shape memory alloys (SMAs) [1–6]. The origin of these effects is the reversible crystallographic transformation between the high-temperature austenite phase B2 (space group: *Pm3m*) and the low-temperature martensite phase B19' (space group: *P2₁m*) [7–9]. Because the B2 ↔ B19' phase transformation temperatures are usually below 100 °C for most Ni–Ti alloys, actual application of these alloys have been limited to below 100 °C [7]. However, many engineering applications of SMAs, particularly in aircraft and automobile engines, as well as

in sensors and actuators in power plants, require the shape memory effect at temperatures higher than 150 °C [9]. For this reason, many researchers have tried to develop a material that can exhibit a shape memory response at high temperatures above 150 °C [5]. It is well known that substituting hafnium (Hf) for titanium (Ti) in a binary Ni–Ti alloy can increase the phase transformation temperature up to 400 °C [10]. The addition of Hf also has advantages over other elements such as Au, Pt, Pd, Nb, and Zr because of its relatively lower cost and reasonably high transformation temperature. However, to date, ternary Ni–Ti–Hf SMAs have not been successfully manufactured into thin wires or sheets on an industrial scale because of the addition of Hf to binary Ni–Ti changes not only the phase transformation temperature but also the deformation characteristics, which results in very poor formability. The hot working of ternary Ni–Ti–Hf SMAs into such forms by means of forging, rolling, and drawing is very difficult because of the formation of a brittle (Ti,Hf)₂Ni phase [11]. To the best of our knowledge, the diameter of the thinnest wire developed so far is ~ 0.75 mm, which is not enough for a fast response time of 1 Hz [12].

On the other hand, pack cementation (PC) is a kind of chemical vapour deposition process that is similar to diffusion coating [13–15]. It is a low-cost process particularly suited for the formation of uniform diffusion coatings on

Electronic supplementary material The online version of this article (<https://doi.org/10.1007/s10973-017-6931-y>) contains supplementary material, which is available to authorized users.

✉ Jeoung Han Kim
jh.kim@hanbat.ac.kr

- ¹ School of Mechanical Engineering, Korea University of Technology and Education, Chonan, Korea
- ² Department of Materials Science and Engineering, Hanbat National University, Daejeon, South Korea
- ³ Titanium Department, Korea Institute of Materials Science, Changwon, South Korea

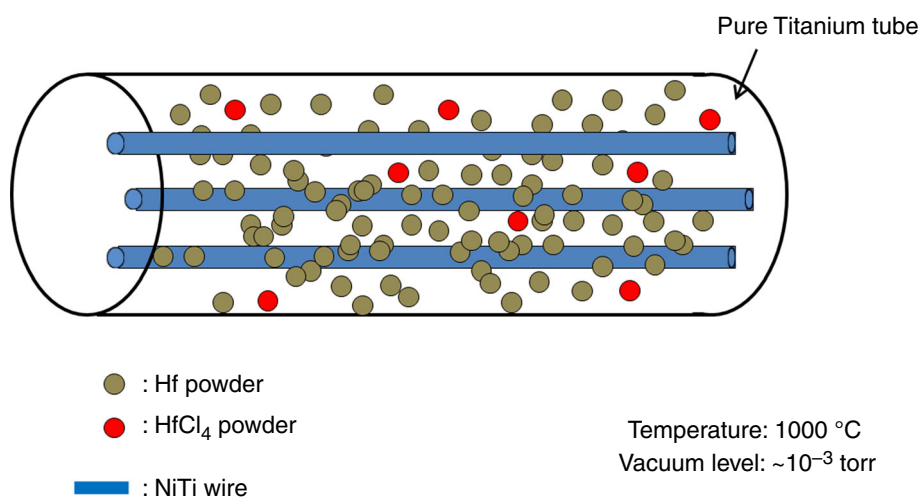
structural alloy components of complex shapes and various sizes [14]. In general, PC is carried out by heating the base material in contact with the powder coating material in an inert atmosphere (solid-state diffusion). It is known that PC can induce the internal diffusion of the coating material to a depth of several hundreds of micrometres. Accordingly, it is possible that a binary Ni–Ti wire with a sufficiently thin diameter can be alloyed with Hf by PC. In a previous work [5], binary Ni–Ti wires with diameters of 0.2 mm were PC treated with Hf powder at 950 °C for 24, 48, and 100 h, and noticeable Hf diffusion into the Ni–Ti wire was observed. However, the diffusion depth was very low, and the increase of the phase transformation temperature was marginal, increasing by only 35 °C. In the present work, a HfCl₄ halide was added as an activator to the PC process to improve the PC effect. HfCl₄ is an inorganic compound with a melting point of 432 °C. It is usually used as a precursor to most hafnium organometallic compounds. During the PC process, the halide activator decomposes and forms metal chloride gases with the diffusing element. The metal chlorides diffuse into the substrate (gas-phase diffusion) and dissociate at the substrate surface. The diffusing element (Hf) is then effectively released and diffuses into the Ni–Ti substrate by solid-state diffusion [15]. Because the halide activator seems to be very effective, in the present work, the feasibility of a halide-activated pack cementation (HAPC) process for the fabrication of a thin Ni–Ti–Hf wire was assessed. After HAPC treatment, careful thermocalorimetric and microstructural analyses were conducted. Also, the Hf diffusion kinetics were studied by establishing a numerical model.

Experimental

The studied 50.4 at.% Ni–Ti-based wires (diameter of approximately 0.5 mm) were provided by Memory Corporation (Connecticut, USA). Before testing, the Ni–Ti surfaces were chemically etched in HF + HNO₃ aqueous solutions for 10 min to remove the initial oxide scales. For the diffusion of Hf into the Ni–Ti wire, the HAPC technique was employed. The pack powder consisted of pure Hf powder and a HfCl₄ activator powder. The Hf and HfCl₄ powders were weighed and mixed using predetermined fractions of 5 and 10 wt% HfCl₄. The powder mixtures were loaded in a titanium tube, together with the cleaned Ni–Ti wires. The titanium tube was placed into a quartz tube that was evacuated to $\sim 10^{-3}$ Torr. The prepared quartz tube was annealed at 1000 °C for 24 h. A schematic illustration of the HAPC process is shown in Fig. 1. The process involved deposition of a Hf-rich vapour onto the Ni–Ti wire substrate embedded in the pack mixture at elevated temperatures.

After the HAPC process, the samples were cut perpendicular to the length direction. A JSM-5800 microscope equipped with an energy-dispersive spectroscope (EDS) was used for scanning electron microscopy (SEM) observation of the cross sections and elemental concentration analysis, respectively. To measure the martensite-to-austenite phase transformation temperature, differential scanning calorimetry (DSC) tests were carried out using a Mettler Toledo DSC1 system. The DSC test consisted of bringing a 5.0 mg Ni–Ti sample from 22 to 250 °C, followed by a return to 22 °C with heating and cooling rates of 10 °C min⁻¹. During the DSC sample preparation, whole body of Ni–Ti(Hf) wire was cut perpendicular to the length direction without considering the inner or outer parts of the sample.

Fig. 1 Schematic illustration of HAPC process



For the DSC sampling, the entire wire was cut in the radial direction without considering the inner and outer parts of the sample.

Results and discussion

Microstructure and Hf distribution after HAPC

Cross-sectional images of the HAPC-processed wire are presented in Fig. 2. In the SEM image (Fig. 2a), no distinctive diffusion or oxide layer was observed in the nearby surface region. Some black particles embedded in the matrix were detected, which seemed to have originated from the Ti_2Ni phase that initially precipitated before the HAPC process. Figure 2b, c shows that the particles were Ti-rich and Ni-lean relative to the matrix. The Hf elemental map shown in Fig. 2d demonstrates that Hf effectively diffused into the centre of the Ni–Ti matrix. Homogeneous Hf distribution was identified, but its concentration appeared to be slightly higher in the outer surface region and lower in the central region.

For quantitative analysis, the elemental concentration along the diffusion depth was measured using the SEM–EDS technique. Figure 3 demonstrates the plots of Hf concentration as a function of distance from the surface. It was confirmed that Hf noticeably diffused into the Ni–Ti matrix during pack cementation both with and without the halide activator. However, in the case of no halide activator, the effective Hf diffusion distance was very short, less than 15 μm . In contrast, the addition of 5 wt% $HfCl_4$ dramatically increased the diffusion distance of Hf. The maximum Hf concentration at the outermost surface was approximately 23 at.%. The Hf concentration rapidly decreased as the distance from the surface increased.

However, relatively high Hf concentration above 10 at.% was obtained at a depth of 75 μm . The addition of 10 wt% $HfCl_4$ to the pack powder mixture further increased the Hf diffusion distance. As compared to the 0 and 5 mass% $HfCl_4$ sample, the slope of the Hf concentration versus diffusion distance profile for 10 mass% $HfCl_4$ sample was less steep. Consequently, at the centre region of the Ni–Ti wire, the Hf concentration was above 8 at.%, which clearly demonstrates the effectiveness of HAPC with a halide activator.

Figure 4 displays the SEM image and EDS elemental mappings of the 10 mass% $HfCl_4$ sample. The observation region was 50 μm away from the outermost surface. Many black particles with diameters of 3–10 μm were embedded in the grey matrix. In the EDS mapping analysis, the particles were found to be Ti-rich particles. Detailed point analysis was conducted, and the results are summarised in Table 1. The table shows that the (Ti + Hf) to Ni ratio in

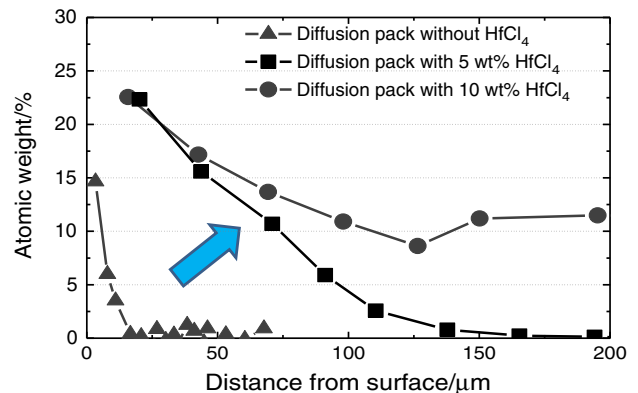


Fig. 3 Composition profiles along the radial direction of the Ni–Ti wire from the surface after HAPC at 1000 °C for 24 h. The weight percentages of the halide activator were 0, 5, and 10 wt%

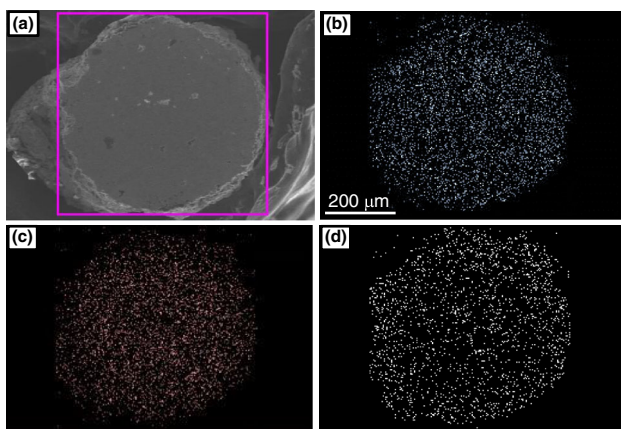


Fig. 2 a SEM microstructure and corresponding energy-dispersive spectrum elemental maps of HAPC-processed Ni–Ti wire; Elemental maps for b Ni, c Ti, and d Hf, respectively

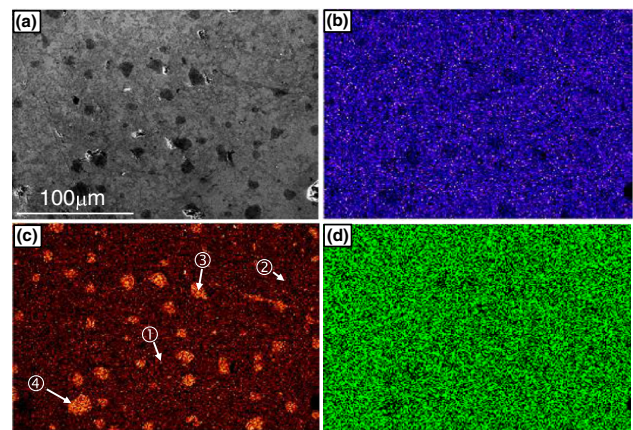


Fig. 4 a Magnified SEM image at 50 μm depth. Corresponding EDS elemental maps of HAPC-processed Ni–Ti wire for b Ni, c Ti, and d Hf. Circled numbers in c indicate the position of EDS analysis in Table 1

Table 1 Chemical composition analysis of the microstructures in Fig. 4

EDS position	Composition/at.%		
	Ti	Ni	Hf
Matrix			
①	35.2	46.9	17.9
②	36.6	46.7	16.7
Particle			
③	57.5	31.6	10.9
④	59.0	32.7	8.3

Circled numbers indicate the position of EDS analysis in Fig. 4c

the black particles is approximately 2:1, which implies that the black particles are $(\text{Ti,Hf})_2\text{Ni}$. The particle size was between 3 and 20 μm , and their volume fraction was approximately 9%. The precipitation of the $(\text{Ti,Hf})_2\text{Ni}$ phase can increase the Ni concentration in surrounding matrix, which leads to the decrease in the transition temperature [16]. Therefore, too much precipitation of a $(\text{Ti,Hf})_2\text{Ni}$ phase is not desirable. On the other hand, the Ti, Ni, and Hf concentrations in the matrix were approximately 35–37, 46–47, and 16–18 at.%, respectively. Generally, a composition of (48–49)Ni–(36–38)Ti–(12–15)Hf is widely found in high-temperature Ni–Ti–Hf SMA studies [9, 17]. Therefore, the matrix composition of the present HAPC-processed sample seems to be acceptable. In 5 mass% HfCl_4 sample, Ti-rich particles with similar particle size were observed too (see Supplementary figure). Interestingly, compared with 10 wt% HfCl_4 , Ni concentration in the matrix was as high as around 51 at.% in the region 50 μm away from the outermost surface. Such high Ni concentration near the surface region may affect phase transformation behaviour. However, the reason for the increase in Ni concentration is not yet clearly understood. It is well known that the phase transition temperature of Ni–Ti SMAs is very sensitive to compositional change. In this regard, more precise composition control would be necessary further.

Differential scanning calorimetry analysis

Figure 5 demonstrates the DSC test results regarding the phase transformation temperatures. Figure 5a shows the DSC curve of the as-received Ni–Ti wire, which exhibits very sharp phase transformation peaks. The martensite-to-austenite transformation start temperature (A_s) was approximately 12 $^{\circ}\text{C}$ and the austenite to martensite transformation start temperature (M_s) was detected at approximately 0 $^{\circ}\text{C}$. Detailed transformation temperatures are summarised in Table 2. These transformation temperatures are close to the typical transformation temperatures

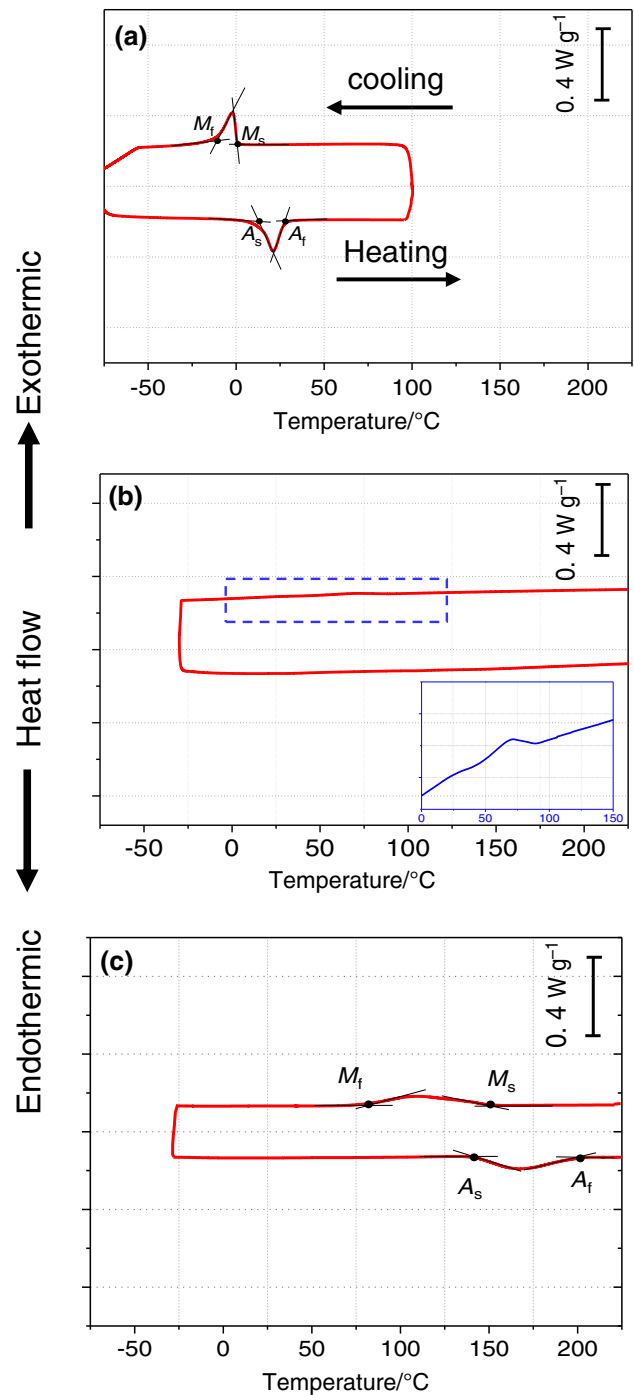


Fig. 5 DSC curves of specimens **a** before HAPC, **b** after HAPC with 5 wt% HfCl_4 , and **c** after HAPC with 10 wt% HfCl_4 for 24 h. M_s , M_f , A_s , and A_f denote martensite start, martensite finish, austenite start, and austenite finish temperatures, respectively

for a Ni-rich binary Ni–Ti system [18]. Unexpectedly, the 5 wt% HfCl_4 addition significantly changed the overall DSC curve, as shown in Fig. 5b. The phase transformation peaks observed in the as-received sample almost disappeared. Instead, small peaks were identified during cooling. A higher magnification image of the area surrounded by the

Table 2 Transformation temperatures, thermal hysteresis, and observed enthalpy change (ΔH) for as-received Ni–Ti and HAPC-treated Ni–Ti

	Transformation temperature/ $^{\circ}\text{C}$				Enthalpy change/ J g^{-1}	
	A_s	A_f	M_s	M_f	$\Delta H^{M \rightarrow A}$	$\Delta H^{A \rightarrow M}$
As-received NiTi	12	28	0	– 10	8.9	7.1
5 wt% HfCl ₄	–	–	89	52	–	–
10 wt% HfCl ₄	142	200	151	82	6.5	6.0

ΔH were calculated simply by integrating the area under the DSC curves in Fig. 5

blue dashed line is shown in the inset in Fig. 5b. The reason for the significant reduction in peak intensity is not well understood. However, it is obvious that the M_s and M_f temperatures increased with the 5 wt% HfCl₄ addition. In contrast, the DSC curve of the Ni–Ti wire after HAPC with 10 wt% HfCl₄ exhibited relatively stronger peak intensities, as demonstrated in Fig. 5c. As compared to the as-received sample, the DSC peaks of the 10 wt% HfCl₄ sample show very low heat flow intensity, and the ranges of the start and finish temperatures are broad. Although the peak sharpness is blurred, the phase transformation temperatures are noticeably higher than those of the as-received Ni–Ti wire. The increased transformation temperature is undoubtedly due to the diffusion of Hf into the Ni–Ti matrix. A diffusion depth of around 200 μm with higher Hf level sufficiently increased the transformation start temperatures by approximately 130–150 $^{\circ}\text{C}$. The phase transformation temperatures are similar to those of typical Ni–Ti SMAs with 10–15 at.% Hf addition [19, 20]. It is thought that some of the Ti in the matrix was replaced by Hf, which resulted in the increase in the transformation temperatures [21].

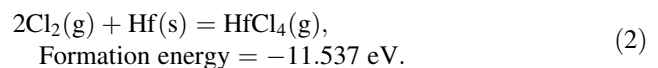
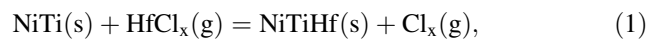
Interestingly, peak broadening was clearly observed in the HAPC samples. This is believed to be the result of a compositional gradient in Hf from the top surface to the core region. The top surface, which has a higher Hf concentration, may exhibit higher phase transformation temperatures, whereas the core region, which has a lower concentration of Hf, may start the phase transformation at lower temperatures. The gradual change in Hf content with increasing distance from the surface may blur the phase transition point. Therefore, the DSC peak is also assumed to change gradually with temperature, resulting in the peak broadening. However, a compositional gradient may not be the only reason for the peak broadening. Tong et al. [21] investigated the effect of Hf content on the DSC behaviour of Ni–Ti–Hf SMAs. In their work, noticeable peak broadening was not observed when the Hf content was below 10 at.%. However, when the Hf content increased to 15 at.%, peak broadening was detected. Unfortunately, the authors did not mention this phenomenon exactly, and thus the reason for the phenomenon is not known. In the present work, outer region of the Ni–Ti wire had a high Hf content

of more than 15 at.%, which is believed to be related to the peak broadening.

Enthalpy changes during the martensite-to-austenite transition ($\Delta H^{M \rightarrow A}$) and vice versa ($\Delta H^{A \rightarrow M}$) were also calculated. As compared to the as-received sample, it was found that HAPC treatment with 10 wt% HfCl₄ addition slightly decreased $\Delta H^{M \rightarrow A}$ from 8.9 and 6.5 J g^{-1} and $\Delta H^{A \rightarrow M}$ from 7.1 and 6.0 J g^{-1} . Generally, the decrease in Ni content in binary Ni–Ti alloys leads to an increase in the volume fraction of the martensite phase, resulting in increased enthalpy changes [18]. However, in the present work, the opposite result was obtained, although the diffusion of Hf to Ni–Ti led to a decrease in the Ni content in the Ni–Ti matrix. Similar results have been reported in Ni–Ti and Ni–Ti–Hf thin films [22]. A possible reason for this is the formation of a relatively high volume fraction of a (Ti, Hf)₂Ni phase, which does not contribute to the martensitic phase transformation.

Hafnium diffusion kinetics

The HAPC method is basically an in situ chemical vapour deposition (CVD) technique because volatile metal-halide vapours are generated during the isothermal coating process by the decomposition of the halide activator (HfCl₄ in this study) [23]. The HAPC process involves following three steps: (1) a gaseous diffusion step (Hf chloride diffuses from the powder pack to the substrate surface), (2) Hf chloride dissociation on the substrate surface, and (3) solid-state Hf diffusion into the Ni–Ti substrate. Reactions steps (2) and (3) can be expressed by the following formula [5, 24, 25]:



Here, solid-state diffusion in the Ni–Ti matrix is assumed to be the rate-limiting step of HAPC. The major Hf-releasing vapour species (HfCl_x gas) that could be generated in the HAPC process is not clear. However, Xiang et al. [14] suggested that the vapour pressures of HfCl and HfCl₂ are always much lower than those of HfCl₃ and HfCl₄. Therefore, it is assumed that HfCl₃ and HfCl₄ are main

vapour species. Unfortunately, reaction energy of $\text{HfCl}_3(\text{g})$ is not available, but its reaction is expected to be similar to that of $\text{HfCl}_4(\text{g})$.

In simulating the above reactions, the weight of the amount of Hf existing in the Ni–Ti wire will depend on the two main mechanisms: the absorption of Hf on the substrate surface and its diffusion into the core of the wire. The first mechanism is represented by the following flux equation:

$$J = h(c_\infty - c), \quad (3)$$

where J is the flux of absorbed atoms on the surface, h is the absorption coefficient, and c_∞ and c are the solubility limit and the concentration of Hf, respectively. This equation serves as the boundary condition on the surface in a differential equation. The second mechanism is simply represented by the Fick's first law of diffusion.

$$J = -D\nabla c, \quad (4)$$

where D is the diffusion coefficient of Hf in the Ni–Ti matrix. It is thought that the greater the amount of HfCl_4 powder added, the greater the gas production and the higher the partial pressure. Consequently, the absorption coefficient and diffusion constant will be functions of the HfCl_4 power amount. In this paper, the finite element method was used to solve the above equations to account for the Hf concentration in the Ni–Ti wire. This type of numerical work can be meaningful for studying the role of each mechanism and estimating the order of magnitude of the material constants. The absorption coefficient (h) and diffusion constant (D) were chosen to fit the experimental results presented in Fig. 3. Figure 6 displays the finite element model used in this work. Only one-quarter of the wire was considered by symmetry. Figure 7 displays the numerically calculated Hf concentration after 24-h annealing for various HfCl_4 amounts. The calculated level of Hf concentration is in good agreement with the

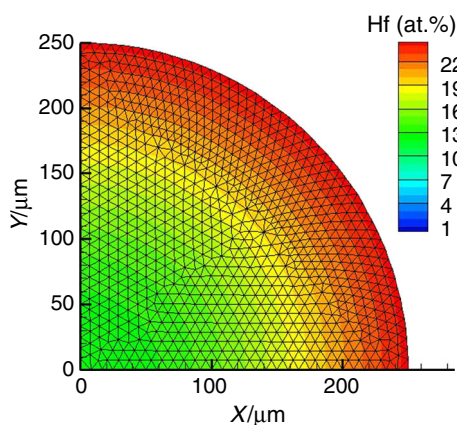


Fig. 6 Hf concentration in Ni–Ti wire cross section after 24 h of HAPC

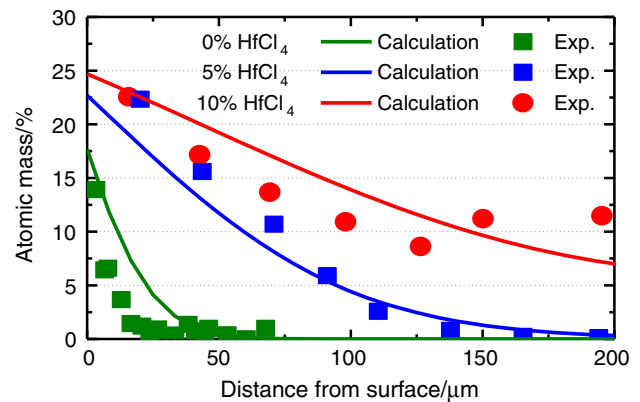


Fig. 7 Calculated Hf concentration profiles along the radial direction after pack cementation for 24 h

experimental results. In the present calculation, the solubility limit was assumed to be constant at $c_\infty = 25 \text{ at.}\%$ [5] and other input parameters were chosen differently for the three HfCl_4 amounts, as listed in Table 3. It is noted that the values of absorption coefficient and diffusion coefficient significantly increased with the addition of HfCl_4 . The D value for the sample without HfCl_4 falls between those of Hf in $\alpha\text{-Ti}$ and pure Ni ($1.1 \times 10^{-17} \text{ m}^2 \text{ s}^{-1}$ at $872 \text{ }^\circ\text{C}$ [26] and $1.2 \times 10^{-15} \text{ m}^2 \text{ s}^{-1}$ at $1050 \text{ }^\circ\text{C}$ [27], respectively). The 5 and 10 mass% HfCl_4 additions exhibited slightly higher diffusion coefficients but not very different. In contrast, the absorption coefficient was considerably dependent on the HfCl_4 amount. The reason for the accelerated absorption rate with HfCl_4 is not clearly understood. It may be because the area in which the Hf transfers from $\text{HfCl}_x(\text{gas})$ to solid Ni–Ti takes place increases with increasing halide addition. As shown in Fig. 8, the entire surface of the Ni–Ti wire is not in contact with the Hf powder. Therefore, the adsorption rate must have been low. In the case of the HAPC-treated Ni–Ti wire, the non-contact area with Hf powder was exposed to $\text{HfCl}_x(\text{gas})$, and thus Hf transfer took place across the whole surface area. The diffusion parameters were effectively dependent on the initial fraction of HfCl_4 powder because the partial pressure of HfCl_3 and HfCl_4 gas increased with the increasing initial addition of HfCl_4 powder.

The Hf concentration profiles after annealing for 48 h were predicted based on the diffusion parameters in Table 3. Figure 9 indicates that little increase in Hf concentration is expected for the 0 mass% HfCl_4 sample as compared to the sample after 24 h of PC. In contrast, the 10 mass% HfCl_4 sample is expected to have a much higher Hf concentration, above 15 at.%. Also, the decrease in Hf concentration along the radial direction is more moderate. Because the peak broadening in the DSC curve is thought to be due to the inhomogeneous Hf concentration

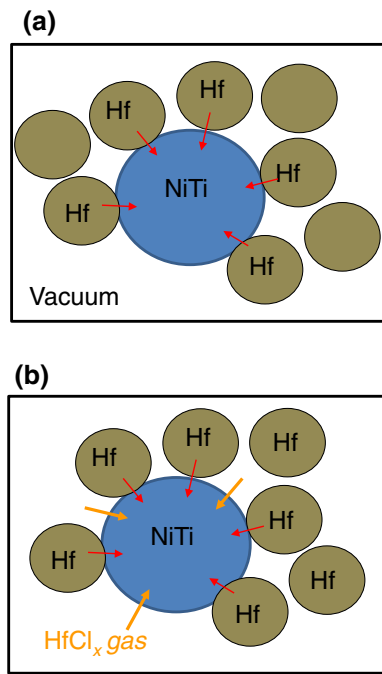


Fig. 8 Schematic diagram explaining the increase in contact area between the Ni–Ti wire and Hf transfer species with halide activator. **a** Without halide activator, **b** with halide activator

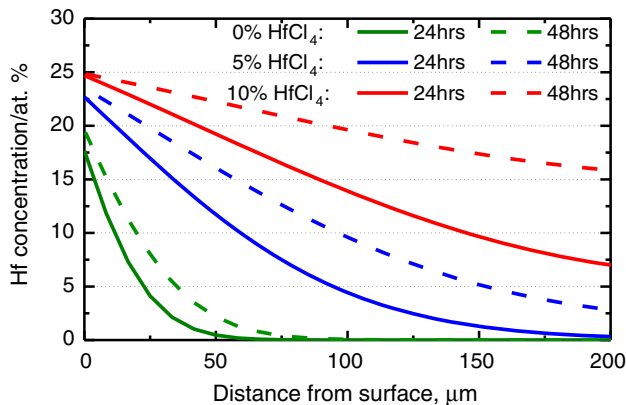


Fig. 9 Calculated Hf concentration profiles along the radial direction after pack cementation for 24 and 48 h

Table 3 Different values of the numerical parameters for different HfCl₄ percentages

	Absorption coefficient, $h/m\ s^{-1}$	Diffusion constant, $D/m^2\ s^{-1}$
Without HfCl ₄	0.001	3×10^{-15}
5 mass% HfCl ₄	0.01	3×10^{-14}
10 mass% HfCl ₄	0.1	9×10^{-14}

throughout the material, the occurrence of a sharper peak is expected with longer HAPC processing times.

Conclusions

1. A Ni–Ti alloy thin wire with a diameter of $\sim 500\ \mu\text{m}$ was pack cemented with Hf powder. Noticeable Hf diffusion into the Ni–Ti wire was observed.
2. A considerable increase in the martensite-to-austenite transformation temperature was found after 24 h of pack cementation. The addition of a HfCl₄ activator significantly increased the diffusion depth of Hf, as well as the phase transformation temperatures. However, only a slight decrease in enthalpy was observed.
3. Hf diffusion kinetics were studied using Fick’s law of diffusion. The absorption coefficient of Hf on the surface of the Ni–Ti wire considerably increased with the addition of the halide activator, whereas the diffusion coefficient was less sensitive to the halide activator.
4. It was predicted that 48 h of HAPC with 10 wt% of HfCl₄ powder is necessary to increase the overall Hf content above 15 at.% throughout the Ni–Ti wire.

References

1. Saud SN, Hamzah E, Abubakar T, Bakhsheshi-Rad HR, Hosseinian R. X-phase precipitation in aging of Cu–Al–Ni–xTi shape memory alloys and its influence on phase transition behavior. *J Therm Anal Calorim.* 2016;123:377–89.
2. El-Bagoury N. Comparative study on microstructure and martensitic transformation of aged Ni-rich NiTi and NiTiCo shape memory alloys. *Met Mater Int.* 2016;22:468–73.
3. Kim JH, Kim KM, Yeom JT, Young S. Effect of yttrium on martensite-austenite phase transformation temperatures and high temperature oxidation kinetics of Ti–Ni–Hf high-temperature shape memory alloys. *Met Mater Int.* 2016;22:204–8. <https://doi.org/10.1007/s12540-016-5130-x>.
4. Choi S-W, Lee H-S, Jeon Y-M, Nam T-H, Yeom J-T, Kim S-W, et al. Effect of chemical composition on the microstructure and high-temperature properties of Ti–Ni–Hf high-temperature shape memory alloys. *J Korean Inst Met Mater.* 2015;53:151–61.
5. Young S, Yeom JT, Hong JK, Kim JH. Diffusion pack cementation of Hf powders on Ni–Ti shape memory alloys. *Sci Adv Mater.* 2016;8:1923–6. <https://doi.org/10.1166/sam.2016.2888>.
6. Antunes AS, Tosetti JPV, Otubo J. High shape recovery Ni–Ti SMA wire produced from electron beam melted ingot. *J Alloys Compd.* 2013;577:S265–7. <https://doi.org/10.1016/j.jallcom.2012.03.043>.
7. Reyes-Melo ME, Rentería-Baltirrez FY, López-Walle B, López-Cuellar E, de Araujo CJ. Application of fractional calculus to modeling the dynamic mechanical analysis of a NiTi SMA ribbon. *J Therm Anal Calorim.* 2016;126:593–9.
8. Torra V, Martorell F, Sun QP, Ahadi A, Lovey FC, Sade M. Metastable effects on martensitic transformation in SMAs: part X. An approach to thermodynamic changes induced for the S-shaped cycles in thick wires of NiTi. *J Therm Anal Calorim.* 2017;128:259–70.

9. Suresh KS, Kim D-I, Bhaumik SK, Suwas S. Evolution of microstructure and texture in Ni_{49.4}Ti_{38.6}Hf₁₂ shape memory alloy during hot rolling. *Intermetallics*. 2013;42:1–8.
10. Stebner AP, Bigelow GS, Yang J, Shukla DP, Saghaian SM, Rogers R, et al. Transformation strains and temperatures of a nickel–titanium–hafnium high temperature shape memory alloy. *Acta Mater*. 2014;76:40–53. <https://doi.org/10.1016/j.actamat.2014.04.071>.
11. Kim DH, Lee YH, Kim JH. Effect of second aging treatment on the microstructure and mechanical properties of SUH660 alloy. *Korean J Met Mater*. 2016;667:311–6.
12. Canadinc D, Trehern W, Ozcan H, Hayrettin C, Karakoc O, Karaman I, et al. On the deformation response and cyclic stability of Ni 50 Ti 35 Hf 15 high temperature shape memory alloy wires. *Scr Mater*. 2017;135:92–6.
13. Park JS, Kim JM, Kim HY, Lee JS, Oh IH, Kang CS. Surface protection effect of diffusion pack cementation process by Al–Si powders with chloride activator on magnesium and its alloys. *Mater Trans*. 2008;49:1048–51.
14. Xiang ZD, Datta PK. Conditions for pack codeposition of Al and Hf on nickel-base superalloys. *Surf Coatings Technol*. 2004;179:95–102.
15. Naji A, Galetz MC, Schütze M. Design model for diffusion coatings formed via pack cementation. *Mater Corros*. 2014;65:312–8. <https://doi.org/10.1002/maco.201307393>.
16. Zarinejad M, Liu Y, Tong Y. Transformation temperature changes due to second phase precipitation in NiTi-based shape memory alloys. *Intermetallics*. 2009;17:914–9. <https://doi.org/10.1016/j.intermet.2009.03.022>.
17. Belbasi M, Salehi MT, Mousavi SAAA, Ebrahimi SM. A study on the mechanical behavior and microstructure of NiTiHf shape memory alloy under hot deformation. *Mater Sci Eng A*. 2013;560:96–102. <https://doi.org/10.1016/j.msea.2012.09.039>.
18. Khalil-Allafi J, Amin-Ahmadi B. The effect of chemical composition on enthalpy and entropy changes of martensitic transformations in binary NiTi shape memory alloys. *J Alloys Compd*. 2009;487:363–6.
19. Thoma PE, Boehm JJ. Effect of composition on the amount of second phase and transformation temperatures of Ni_xTi_{90-x}Hf₁₀ shape memory alloys. *Mater Sci Eng, A*. 1999;275:385–9.
20. Firstov GS, Van Humbeeck J, Koval YN. High-temperature shape memory alloys some recent developments. *Mater Sci Eng A*. 2004;378:2–10.
21. Tong Y, Chen F, Tian B, Li L, Zheng Y. Microstructure and martensitic transformation of Ti₄₉Ni_{51-x}Hf_x high temperature shape memory alloys. *Mater Lett*. 2009;63:1869–71. <https://doi.org/10.1016/j.matlet.2009.05.069>.
22. Rao J, Roberts T, Lawson K, Nicholls J. Nickel titanium and nickel titanium hafnium shape memory alloy thin films. *Surf Coatings Technol*. 2010;204:2331–6. <https://doi.org/10.1016/j.surfcoat.2009.12.025>.
23. Cheng J, Yi S, Park JS. Simultaneous coating of Si and B on Nb–Si–B alloys by a halide activated pack cementation method and oxidation behaviors of the alloys with coatings at 1100 °C. *J Alloys Compd*. 2015;644:975–81. <https://doi.org/10.1016/j.jallcom.2015.05.003>.
24. The Materials Project. Reaction Calculator. https://www.materialsproject.org/apps/reaction_calculator/.
25. Fridman A. Plasma chemistry. New York: Cambridge University Press; 2008.
26. Pérez RA, Dymont F, Bermúdez GG, Somacal H, Abriola D. Measurements of Hf diffusion in α -Ti by HIRBS. *J Nucl Mater*. 1993;207:221–7.
27. Shuwei MA, Yunrong Z. Diffusion behaviour of hafnium in Ni and Ni₃Al. *J Mater Sci Lett*. 1997;6:1761–3.